Chirality Sensing

Tandem Use of Optical Sensing and Machine Learning for the Determination of Absolute Configuration, Enantiomeric and Diastereomeric Ratios, and Concentration of Chiral Samples

Zeus A. De los Santos, Sean MacAvaney, Katina Russell, and Christian Wolf*

Abstract: We have developed an optical method for accurate concentration, er, and dr analysis of amino alcohols based on a simple mix-and-measure workflow that is fully adaptable to multiwell plate technology and microscale analysis. The conversion of the four aminoindanol stereoisomers with salicylaldehyde to the corresponding Schiff base allows analysis of the dr based on a change in the UV maximum at 420 nm that is very different for the homo- and heterochiral diastereomers and of the concentration of the sample using a hypsochromic shift of another absorption band around 340 nm that is independent of the analyte stereochemistry. Subsequent in situ formation of Cu^{II} assemblies in the absence and presence of base enables quantification of the er values for each diastereomeric pair by CD analysis. Applying a linear programming method and a parameter sweep algorithm, we determined the concentration and relative amounts of each of the four stereoisomers in 20 samples of vastly different stereoisomeric compositions with an averaged absolute percent error of 1.7%.

Introduction

The advance of high-throughput strategies and the introduction of commercially available instrumentation capable of parallel analysis of large numbers of microscale samples have greatly accelerated R&D productivity across the chemical, materials, and life sciences during the last decade.[1] The progress with scientific discoveries or process development tasks, however, is often slowed down or even stalled when the analysis of the concentration and the enantiomeric composition of hundreds to thousands of chiral samples is required.[2] To date, the determination of the enantiomeric ratio (er) of chiral analytes is typically accomplished with chromatographic techniques that are intrinsically serial, time-consuming and produce large amounts of solvent waste, albeit high-speed HPLC and SFC separations have recently been reported.[3] Alternatively, mass spectrometry,[4] IR thermog-

raphy,[5] NMR spectroscopy,[6] capillary electrophoresis,[7] and biochemical assays[8] have been used to quantify enantiomeric mixtures.

To address the limited capacity and lack of throughput with the stereochemical analysis of chiral compounds, a variety of fast and cost-efficient optical sensing assays that are compatible with automation, multiwell plate technology, and parallel screening operations have been developed.[9] Many examples of concurrent concentration and er sensing with fluorescence,[10] UV,[11] and circular dichroism (CD) spectroscopic methods including optical asymmetric reaction analysis have been reported.[13] By contrast, the steadily growing demand for methods that allow determination of the er and the diastereomeric ratio (dr) of compounds exhibiting more than one chiral center, for example in the drug development arena, has been largely neglected. Although an impressive diversity of robust sensor designs is available, the development of optical methods that achieve accurate determination of concentration, er and dr values following a practical workflow is a formidable challenge. Anslyn's and our group have shown that ternary isomeric mixtures containing the enantiomers and the *meso* form of 1,2-diamines can be identified and analyzed either by linear discriminant analysis with a chiral BINAP-Cu^I complex[14] or with a ligand displacement assay using a fluorescent diacri-dylnaphthalene *N,N'*-dioxide scandium(III) complex.[15] Anzenbacher and Pu described optical systems with potential for diastereo- and enantioselective fluorosensing of hydroben-zoin and threonine mixtures, respectively, but the combined quantification of er and dr values was not demonstrated.[16, 13d] The possibility of optical concentration, er, and dr analysis of 2-aminocyclohexanol with a maximum absolute error of 12.7% was recently demonstrated by the Anslyn group using a tandem of UV, CD and fluorescence assays that require protection chemistry, working at elevated temperature, and reaction work-up (extraction, filtration, and solvent removal).[17]

Vicinal amino alcohols are among the most privileged classes of compounds and widely used as key building blocks for the synthesis of biologically active compounds and as chiral ligands or auxiliaries in asymmetric reactions. The evaluation of the total amount and the stereoisomeric composition of chiral amino alcohols is therefore a very important and frequently encountered task. In many cases, the presence of two stereogenic centers gives rise to two diastereomers, each comprising a pair of enantiomers. The determination of the total amount and the relative quantities of the four stereoisomeric forms is typically accomplished by

[*] Z. A. De los Santos, Prof. C. Wolf
Department of Chemistry, Georgetown University
Washington, DC 20057 (USA)
E-mail: cw27@georgetown.edu

S. MacAvaney, K. Russell
Department of Computer Science, Georgetown University
Washington, DC 20057 (USA)

Supporting information and the ORCID identification number(s) for the author(s) of this article can be found under:
https://doi.org/10.1002/anie.201912904.

gravimetric analysis in combination with either chiral chromatography using standard reference samples for comparison or by NMR spectroscopy with chiral solvating agents or derivatizing reagents.[18] As mentioned above, these are inherently serial techniques that are often time-consuming, and when compared to optical sensing approaches, are less amenable to high-throughput screening.
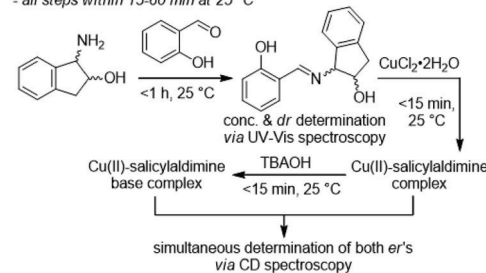
We report herein a method for accurate concentration, *er*, and *dr* analysis of amino alcohols based on machine learning and a simple mix-and-measure workflow that is fully adaptable to multiwell plate technology and applicable to microscale analysis. Conversion of the four aminoindanol stereoisomers with salicylaldehyde to the corresponding Schiff base allows analysis of the diastereomeric composition and the total amount (concentration) of the sample based on a change in the UV maximum absorbance at approximately 420 nm that is the same for the individual enantiomers and a hypsochromic shift of another absorption band around 340 nm that is independent of the analyte stereochemistry. The subsequent in situ formation of Cu^II assemblies in the absence and presence of base enables quantification of the *er* values for each diastereomeric pair by CD analysis at 340–350 nm and 410–420 nm, respectively. Applying a linear programming (LP) method to optimize the weighting of UV/Vis and CD spectra and a parameter sweep (PS) algorithm to identify optimal wavelength ranges for the most accurate and robust analysis using 20 training samples, we determined the percent amounts of each of the four stereoisomers in 20 samples with a maximum absolute error of only 8.0%. Our approach is very practical and offers several advantageous features. Only CD and UV measurements are required, which facilitates the workflow as modern UV/CD instruments and plate readers typically generate both spectra simultaneously. All spectroscopic readouts used for the analysis appear above 300 nm, which is advantageous because this is more likely to eliminate possible interferences from impurities. We avoid neat reaction conditions that might be difficult to handle when minute sample amounts have to be processed, and derivatizations that require heating, which could result in partial solvent loss and concentration alterations that may compromise the accuracy of the optical assay. Protection chemistry and any work-up are also avoided, and all reagents used are commercially available and inexpensive. The Schiff base and Cu^II complex formations are complete within 30 and 15 min, respectively, and occur at 25°C, which greatly facilitates parallel handling of hundreds of samples in a single multiwell plate under uniform temperature conditions if desired (Scheme 1).
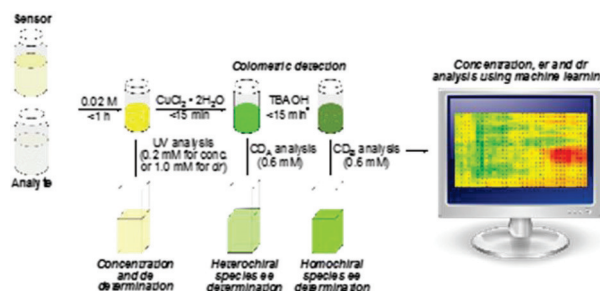
Results and Discussion

The widespread use of high-throughput equipment enables chemists to run hundreds of asymmetric reactions at the 1 milligram scale in parallel to optimize catalyst structure, additives, solvents, or other important parameters. Typically, catalytic reactions are complete within a few hours or overnight and then await evaluation. The remaining bottleneck of the overall development progress, however, com-


Scheme 1. Quantitative optical sensing of mixtures of four stereoisomers of amino alcohols.

monly lies in the analysis of the product yield and *er* for each run because traditional methods are either not applicable to small-scale reactions or time-consuming. While the introduction of optical assays has been shown to solve this problem for reactions that generate compounds with a single chiral center existing only in the form of two enantiomers,[9e] the sensing of mixtures that contain diastereomers, each existing as a pair of enantiomers, remains a major challenge. The discovery and optimization of asymmetric reactions that introduce two chirality centers with high enantio- and diastereoselectivity is a frequently encountered task in numerous laboratories. An analytical method that can handle high-throughput screening of mixtures of enantiomers and diastereomers is therefore in high demand.

At the onset of this study, we envisioned a practical sensing assay that allows differentiation of four stereoisomers and accurate quantification of *er* and *dr* values based on a very attractive mix-and-measure workflow with the following features: 1) It can be applied to minute sample amounts, 2) eliminates any work-up steps, 3) requires only inexpensive, commercially available agents, and 4) would be readily adaptable to high-throughput instrumentation and automated operation. Based on the general significance and ubiquity of amino alcohols described above, we selected aminoindanol, **1**, exhibiting two vicinal chirality centers as test compound. Our group has developed a variety of optical sensing methods that exploit the principles of dynamic covalent chemistry, for example through reversible Schiff base formation,[19] or coordination of a chiral analyte to stereodynamic metal complexes[20] to produce UV and CD spectra that allow the determination of concentration and enantiomeric composi-

tion of a large number of compounds including amino alcohols. We expected that the general practicality and efficiency of these sensing strategies would be highly advantageous in our search for an optical method that achieves comprehensive stereoselective analysis of **1** while adhering to the unique features itemized above.

After screening several Schiff base sensor designs and conditions, we found that the diastereomers of **1** react quantitatively with salicylaldehyde **2**, to the corresponding homo- and heterochiral imines **3**, which have optical properties that are favourable for quantitative sensing (Scheme 2).
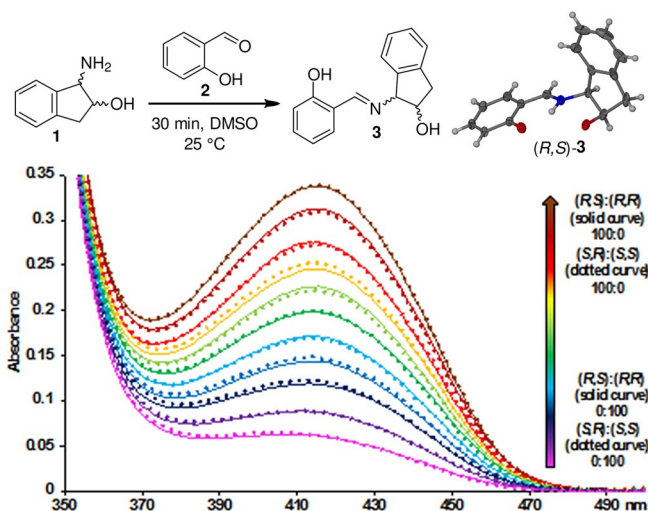
Scheme 2. Schiff base formation and diastereoselective UV sensing. UV/Vis spectra of the salicylaldimine formed from **1** and **2** at varying *dr* starting from 100 mol% of either (*R*,*R*)-**1** (solid magenta curve) or (*S*,*S*)-**1** (dotted magenta curve) to 100 mol% of either (*R*,*S*)-**1** (solid brown curve) or (*S*,*R*)-**1** (dotted brown curve). All UV spectra were recorded at a concentration of 1.0 mM in DMSO.

The condensation reaction occurs smoothly under stoichiometric conditions in DMSO at room temperature and is complete within 30 min according to UV analysis. Formation of by-products that could potentially interfere with the chiroptical sensing was excluded by NMR and IR spectroscopy and ESI-MS (Supporting Information). To assure high reproducibility of our sensing assay we allowed a 1-hour reaction time for all experiments. Further analysis revealed that the UV spectra of the salicylaldimine enantiomers formed from **1** are identical as one would expect. However, the signal intensity at 415 nm increases substantially as the relative amount of the homochiral diastereomer, that is, (*R*,*R*)-**3** and (*S*,*S*)-**3**), versus the heterochiral diastereomer, (*R*,*S*)-**3** and (*S*,*R*)-**3**), decreases. The steady change in the UV absorption intensity can therefore be used to determine the *dr* of samples of **1**.

We recently reported that chiroptical analysis of unprotected chiral amino alcohols and many other classes of compounds is possible with a simple mix-and-measure protocol using inexpensive cobalt, iron, copper, and other metal salts that generate strong Cotton effects at long wavelengths.[21] The induced CD (ICD) signals were successfully correlated to the enantiomeric ratio of the sensing targets and used for quantitative *er* determination. These findings encouraged us to examine the possibility of using metal complexation of **3** for the same purpose.

The testing of various metal salts and optimization of the analyte-to-metal-ion ratio revealed very strong CD effects, in particular when 0.5 equivalents of copper(II) chloride were employed (Figure 1 and the Supporting Information). The complex formation is fast and coincides with a characteristic change from pale yellow to green and dark yellow when the heterochiral and homochiral imines, respectively, are added. The CD spectra can be collected within 15 min. A closer inspection of the ICD effects showed distinct Cotton effects
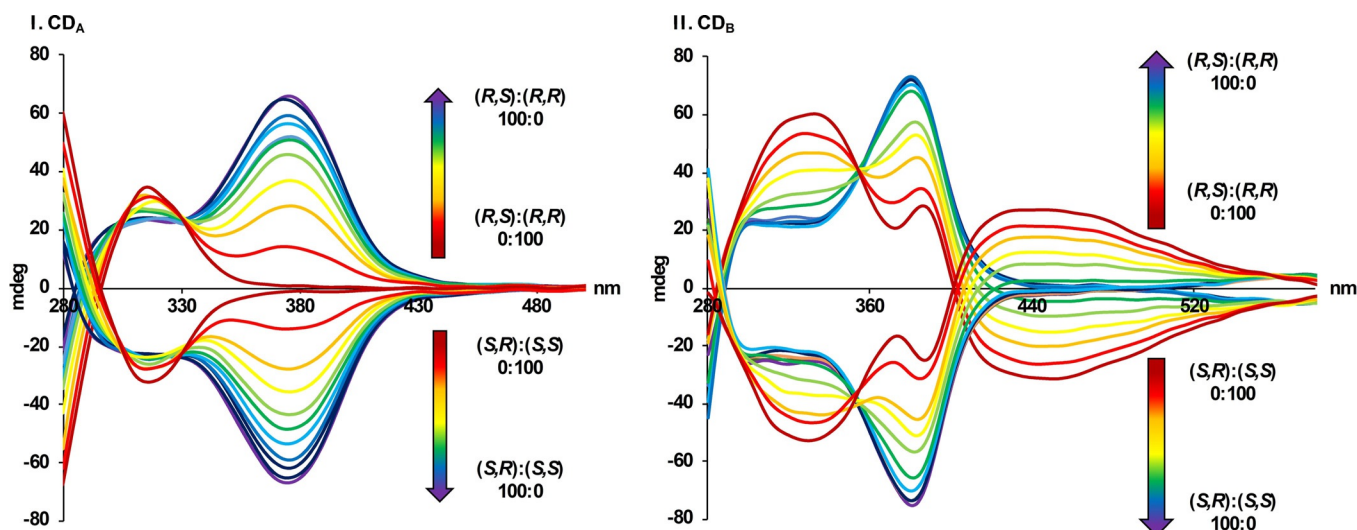
Figure 1. CD spectra of the Cu^{II} assemblies formed from salicylaldimine **3** and 0.5 equiv of CuCl$_2$·2H$_2$O (left, CD$_A$) and after addition of 1 equiv of TBAOH (right, CD$_B$). Gradation of color from maroon to purple indicates distribution of *dr* between homochiral (i.e., maroon is either 100% (*R*,*R*)- or 100% (*S*,*S*)-**1**) and heterochiral (i.e., purple is either 100% (*R*,*S*)- or 100% (*S*,*R*)-**1**) species. CD analysis was performed at a concentration of 0.6 mM in DMSO.

for all four stereoisomers. A strong positive signal at approximately 380 nm appears in the presence of the (*R*,*S*)-enantiomer, while the exact opposite curvature with a strong negative CD maximum at the same wavelength is observed with the (*S*,*R*)-enantiomer (CD$_A$, purple curves). By contrast, the Cu^{II} complexes of the homochiral enantiomers are CD-silent at 380 nm but display a maximum around 320 nm, which is positive for the (*R*,*R*)-enantiomer and negative for its antipode (CD$_A$, maroon curves). The effect of a gradual change in the *dr* of the Schiff base, for example from the (*R*,*R*)-imine copper complex to the (*R*,*S*)-analogue, is visualized by the color change from maroon to purple. Moreover, we observed a dramatic CD modulation upon addition of base. Again, the system equilibration and subsequent chiroptical changes are very fast and we were able to conduct all CD experiments without delay. In the presence of 1 equivalent of tetrabutylammonium hydroxide (TBAOH), the CD spectra of the heterochiral complexes remain quite similar (CD$_B$, purple curves). The homochiral Cu^{II} complexes, however, give strikingly different results. The (*R*,*R*)-imine copper assembly now shows a positive CD maximum at approximately 440 nm and two negative peaks between 300 and 400 nm. As expected, the opposite effects are observed with the (*S*,*S*)-enantiomer (CD$_B$, maroon curves). The same CD modulation effects were obtained when TBAOH was replaced with KOH or diisopropylethylamine (Supporting Information).

Based on the detailed studies of chiroptically active metal ion assemblies previously communicated from our laboratory,[21] the measured ICD signals generated upon addition of CuCl$_2$·2H$_2$O to solutions of the imine **3** are likely attributable to a complex mixture of enantiomeric and diastereomeric copper complexes that are in equilibrium with multinuclear species. In fact, we were able to identify both dinuclear and trinuclear copper complexes of **3** by ESI-MS, which is in agreement with the X-ray structure of a single crystal obtained by slow evaporation of a methanol solution of the heterochiral Schiff base and CuCl$_2$ (Figure 2 and Supporting Information). Our spectroscopic and crystallographic observations are in accordance with a wealth of studies and thorough characterizations of copper complexes carrying amino-alcohol-derived Schiff base ligands.[22] The well-documented complicated nature of such Cu^{II} complexes and their aptitude to form multinuclear species, however, have not impeded their successful use in asymmetric catalysis;[23] and as
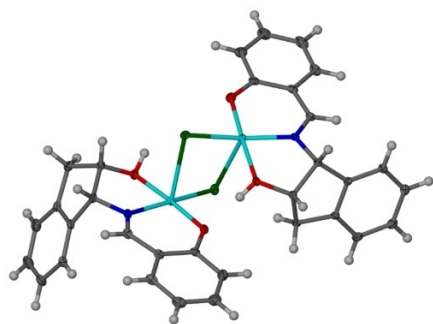
we show in this work, these features do not affect the efficiency and practicality of quantitative *er*/*dr* sensing.

Having developed a simple workflow that yields characteristic UV and CD readouts of the four stereosiomers of **1** upon Schiff base formation, copper coordination, and base addition, we continued with the analysis of our sensing results. To accomplish the quantification of the large body of data, we referred to a supervised learning approach based on linear programming (LP). LP is a class of optimization algorithm that finds an optimal result with minimal deviation from the actual value, subject to several constraining variables. In this study, LP is employed to find the combination of UV/Vis and CD calibration curves that minimizes the squared distance between an unknown value (i.e., concentration, *dr*, or *er*) across various wavelength ranges. The algorithm exploits areas in which one species gives a predominant spectroscopic output to generate weights for each calibration curve (blue, green, orange, and red lines in Figure 3) such that, when combined, a computed spectrum (pink dashed line) that is superimposable onto the target spectrum (black dashed line) is obtained. The weights for each calibration curve are then employed to predict the composition of unknown samples by weighting the composition of each calibration curve (Supporting Information).

We realized that manual identification of regions in which quantitative differentiation between the four stereoisomeric species is optimal can be time-consuming, prone to errors, and generate unnecessary bias. This important task was therefore achieved by using a parameter sweep (PS) algorithm. PS uses a set of training samples with known compositions of quaternary isomeric mixtures of **1** to identify the wavelength ranges that the algorithm can use to ensure efficient and accurate analysis. For this purpose, a training set composed of 20 samples, **T1**–**T20**, with varying *dr* and *er* of aminoindanol was prepared and the UV/Vis and CD spectra were collected according to the procedure described above (see the Supporting Information for details). The spectra obtained were then fed into the LP algorithm to obtain individual percent compositions of (*R*,*S*)-**1**, (*S*,*R*)-**1**, (*R*,*R*)-**1**, (*S*,*S*)-**1** (*er* values), and [(*R*,*S*)-**1** + (*S*,*R*)-**1**] and [(*R*,*R*)-**1** + (*S*,*S*)-**1**] (*dr* values). First, the results for each training sample obtained from all possible 10, 50, 100, 150, and 200 nm ranges were evaluated by 10 nm steps across the whole spectrum width (i.e., 280–600 nm). Then, the optimal wavelength span was selected by identifying the range that produces the lowest averaged absolute error across all composition (concentration, *dr*, and *er*) values. This process is completely automated and can be executed in about one hour.

The distribution of the averaged absolute errors across 20 samples from the training set within the 10 nm segments between 280 nm to 600 nm is shown in Table 1. The color scheme shows gradation among the calculated averaged absolute %error indicating an increase from green to red (i.e., values having lowest percent error are in green and values having highest %error are in red). The wavelength range that gives the lowest averaged absolute percent error of only 1.2% is highlighted in a red box. The averaged absolute percent error is defined as the error obtained from comparing *er* and *dr* values using LP against actual values across all 20
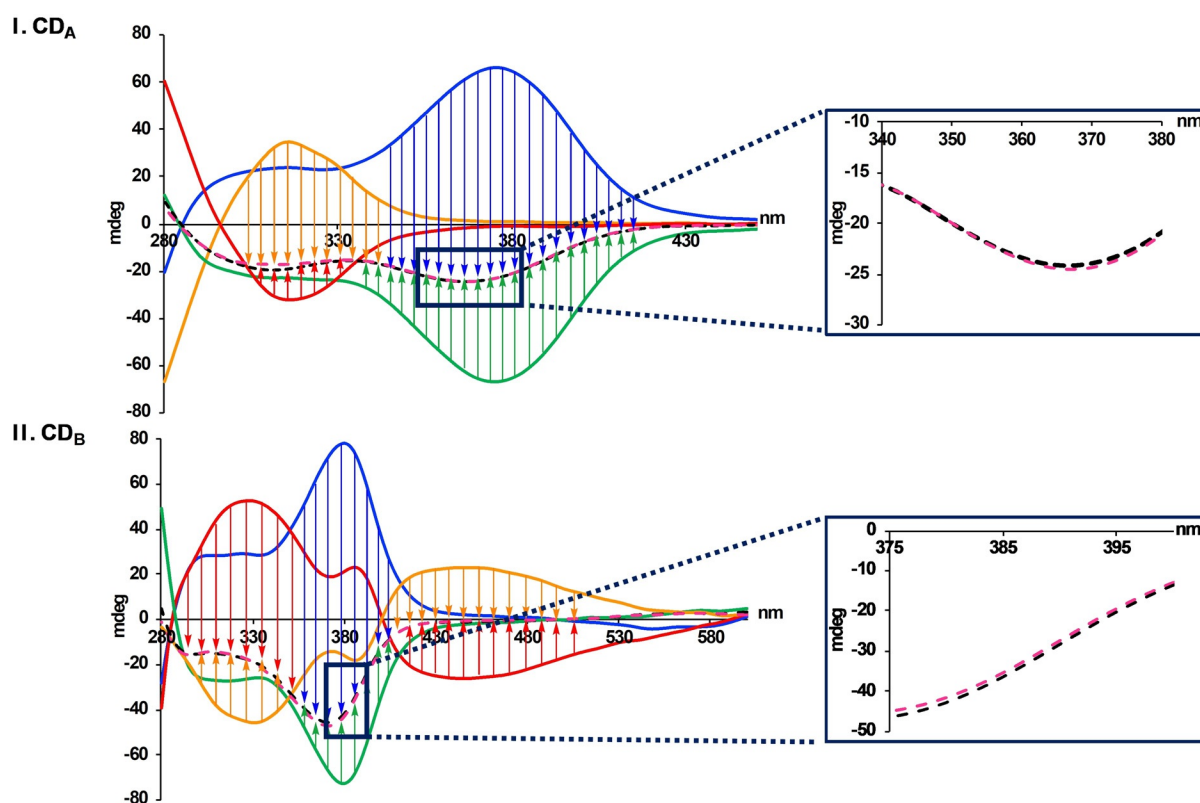

Figure 2. Single-crystal structure of [Cu(*R*,*S*)-**3**]$_2$.[24]

Figure 3. CD_A (top) and CD_B (bottom) spectra of the assemblies formed between Cu^{II}, enantiopure (R,S)-**3** (blue), (S,R)-**3** (green), (R,R)-**3** (orange), and (S,S)-**3** (red) (CD_A), and after addition of one equivalent of TBAOH (CD_B). The LP algorithm is employed to find a set of weights to minimize the squared distance between the experimental curve (dashed black line) from different calibration curves across various wavelength ranges. Insets: The experimental curves (dashed black curve) of sample **S2** (Table 2) and the calculated curves from LP (pink dashed curve) are superimposable.

samples in the training set. The results obtained with wavelength segments of 50, 100, 150, and 200 nm are tabulated in the Supporting Information.

The PS analysis of our training set suggested that the 340–350 nm (CD_A) and 410–420 (CD_B) segments are optimal for the chiroptical analysis of stereoisomeric mixtures of **1**. To test the accuracy of our method, we prepared twenty scalemic mixtures of **S1**–**S20** with substantially varying *dr* and *er* values. The samples were treated following our general sensing workflow. The experimentally obtained UV and CD spectra were fed into the LP algorithm, and by using the optimized ranges, the individual amounts of all four stereoisomers of **1** were calculated. The results are shown in Table 2. Comparisons of the experimentally obtained and the LP-generated CD_A and CD_B spectra showing excellent agreement in the 10 nm regions selected by our supervised learning approach can be found in Figure 3 and in the Supporting Information.

The stereoselective determination of the concentrations and relative amounts of the four stereoisomers as well as the correct assignment of the absolute configuration of each individual component was accomplished with excellent accuracy for all 20 samples. For example, the *er* and *dr* sensing of **S2** consisting of 31% (69%) of the heterochiral (homochiral) amino alcohol and 5.0%, 26.0%, 8.3% and 60.7% of (R,S)-, (S,R)-, (R,R)- and (S,S)-**1**, respectively, gave the same diastereomeric composition while the individual isomers

were calculated as 3.1%, 27.9%, 8.7% and 60.3%, respectively. A comparison with the results obtained for **S4** demonstrates that the method is broadly reliable as significant changes in the enantiomeric and diastereomeric compositions are not a problem. In this case, the quantification of a 91:9 *dr* mixture containing the (R,S)-, (S,R)-, (R,R)-, and (S,S)-isomers in 81.9%, 9.1%, 7.6%, and 1.4% gave a *dr* of 90:10 and individual percentages of 79.8, 10.2, 7.9, and 2.1, respectively. Overall, we were able to determine the percent amounts of each of the four stereoisomers in the 20 samples with an averaged absolute percent error of only 1.7%. The maximum absolute error in **S1**–**S20** was determined as 8.0% (see **S9** in Table 2).

Further examination of our sensing results showed that the UV spectra obtained with the salicylaldimine **3** contain a region between 330 and 350 nm that can be used for concentration analysis independent of the enantiomeric and diastereomeric sample composition. We found that a hypsochromic shift and a decrease in signal intensity are observed as the concentration of **1** increases (Figure 4). The Schiff bases formed from the individual enantiomers and diastereomers of **1** and sensor **2** produce almost perfectly superimposable UV responses between 338 to 345 nm, which allows concentration determination of the analyte. To demonstrate the viability of the concentration analysis, seven samples of varying concentrations (6.0–15.0 mM) of **1** were prepared according to our

Table 1: PS-generated averaged absolute percent error distribution across 20 training set samples **T1**–**T20** within 10 nm segments between 280 to 600 nm.[a]

CD_A	280	290	300	310	320	330	340	350	360	370	380	390	400	410	420	430	440	450	460	470	480	490	500	510	520	530	540	550	560	570	580	590
CD_B	290	300	310	320	330	340	350	360	370	380	390	400	410	420	430	440	450	460	470	480	490	500	510	520	530	540	550	560	570	580	590	600
280 290	2.2	2.6	5.3	3.5	2.3	2.3	2.1	2.5	2.4	2.5	2.6	2.5	2.4	2.7	3.5	3.6	3.7	4.4	4.9	4.5	5.1	5.6	4.5	4.5	4.4	4.8	4.9	4.0	3.9	4.7	4.6	5.4
290 300	2.8	2.4	4.0	3.4	2.2	2.0	2.3	2.4	2.3	2.5	2.2	2.4	2.4	2.6	3.4	3.2	3.2	4.1	4.5	4.8	5.4	5.2	5.4	6.0	6.0	6.3	7.3	5.8	6.1	5.7	3.8	4.2
300 310	2.8	3.3	3.4	3.5	2.5	2.3	1.9	2.5	2.3	2.6	2.1	2.3	2.1	2.1	2.9	2.8	3.3	3.2	4.1	3.5	3.7	3.4	4.4	3.7	3.3	4.2	5.5	4.6	5.1	4.7	4.0	4.5
310 320	3.2	3.4	4.8	3.2	2.5	2.3	2.1	2.8	2.8	2.6	2.8	3.0	3.2	3.0	3.4	3.6	3.6	3.2	4.2	5.4	5.9	6.7	6.4	8.7	8.6	7.2	6.1	5.5	5.4	5.7	4.4	6.3
320 330	2.7	2.5	5.3	3.6	2.7	1.9	2.3	2.6	2.4	2.6	2.6	2.4	2.5	2.5	2.6	2.9	2.7	3.1	2.7	3.0	4.4	5.4	5.7	5.4	5.6	5.9	4.7	7.0	6.0	4.0	4.0	4.5
330 340	2.7	3.4	5.6	4.7	3.4	1.8	2.8	2.5	2.9	2.4	2.7	2.0	2.1	2.6	2.6	2.4	2.4	2.5	3.3	2.9	3.2	2.7	3.1	3.3	3.8	3.1	3.5	2.9	3.3	3.6	3.0	3.4
340 350	2.7	3.6	3.3	3.1	3.2	2.4	1.7	3.0	2.2	1.8	2.5	2.3	2.0	2.1	2.4	2.7	2.2	2.2	2.9	2.5	2.3	3.1	2.8	2.9	2.8	2.7	2.5	2.6	2.8	2.9	3.1	3.5
350 360	2.6	2.8	3.8	3.5	2.7	1.7	1.8	3.2	1.9	1.8	1.9	1.4	1.9	2.3	2.6	2.5	2.7	2.5	3.0	2.6	2.4	3.2	2.7	2.3	3.0	3.3	2.9	2.7	2.8	2.7	2.9	3.5
360 370	2.6	2.9	4.1	3.1	3.1	1.3	1.5	2.3	2.7	2.0	2.0	1.8	2.9	2.8	3.1	3.6	3.7	2.6	2.8	2.9	2.5	2.6	2.2	2.3	2.4	2.6	3.4	3.8	3.7	3.5	3.6	4.2
370 380	2.7	2.7	3.4	3.2	3.0	1.7	1.9	3.4	3.3	3.4	3.2	2.3	2.8	3.0	3.5	3.9	3.5	3.4	4.0	3.4	4.0	4.4	5.0	5.1	4.9	5.1	5.6	5.3	4.3	3.9	4.7	6.4
380 390	2.8	2.9	3.8	3.3	2.9	1.7	2.6	4.4	2.1	3.7	3.0	2.1	2.3	2.9	3.0	2.7	3.1	4.4	2.5	2.7	2.5	2.4	2.1	2.1	2.4	2.3	3.4	3.3	3.1	3.2	3.7	4.5
390 400	3.0	2.8	4.0	3.9	3.6	1.7	2.2	2.7	2.1	2.0	3.2	2.0	2.3	2.6	2.9	3.5	2.6	2.0	2.3	2.3	2.1	2.2	2.1	2.1	3.0	3.0	2.1	2.4	2.6	2.6	3.5	4.2
400 410	3.0	3.1	4.4	3.3	2.1	1.4	1.6	2.2	2.5	1.8	2.2	1.8	2.0	2.8	2.8	2.8	2.6	2.1	1.9	2.3	2.1	2.7	2.0	2.1	2.2	3.8	2.4	2.4	2.7	3.5	3.5	3.8
410 420	2.2	2.8	3.0	2.3	2.5	1.7	1.2	2.4	2.0	1.7	1.8	2.0	2.4	1.7	2.5	2.8	2.4	1.8	2.3	1.8	2.1	2.6	2.1	2.9	3.2	3.0	3.4	3.6	4.6	5.0	4.2	5.0
420 430	2.2	2.5	2.4	2.2	2.5	2.0	1.5	2.5	2.1	2.2	2.1	2.6	2.3	2.6	2.6	3.2	2.8	2.4	2.5	2.4	2.3	3.3	2.4	4.3	4.5	7.0	7.9	8.9	7.9	8.9	7.4	6.6
430 440	2.4	2.9	3.2	2.5	2.5	2.1	1.5	2.8	2.4	2.1	3.3	2.7	3.2	3.1	3.0	2.9	3.0	3.5	4.0	4.8	5.5	6.1	6.5	9.8	11.4	11.0	11.6	12.0	10.9	11.6	8.5	7.8
440 450	2.6	2.6	2.7	2.4	2.4	2.7	1.5	2.4	2.4	2.1	2.6	2.5	2.7	2.4	2.4	2.6	2.7	3.8	4.2	4.0	5.3	7.2	8.3	12.2	15.1	14.2	14.0	16.6	13.4	12.9	12.2	9.9
450 460	2.4	3.3	2.8	2.6	2.3	2.0	1.7	3.6	3.1	2.1	2.7	2.6	2.9	2.8	3.0	2.6	2.9	4.4	4.7	3.7	5.1	7.1	7.8	12.3	14.5	14.6	14.8	16.9	14.4	14.3	10.9	10.4
460 470	2.1	2.3	2.3	2.5	2.1	2.0	1.5	2.6	1.8	2.4	2.6	2.6	2.7	2.9	2.4	2.6	2.9	4.1	4.0	3.6	4.1	5.6	6.8	13.4	13.5	13.3	13.4	15.4	11.9	13.1	11.3	11.4
470 480	2.2	2.6	3.1	2.3	2.4	2.3	1.3	2.7	2.8	2.6	2.5	2.6	2.4	2.6	2.3	2.5	2.9	3.9	4.3	4.1	3.7	5.2	7.2	12.8	14.1	12.9	13.5	15.3	12.2	14.2	13.0	11.0
480 490	2.3	2.3	2.9	2.2	2.3	1.9	1.3	2.9	2.3	2.6	2.6	3.2	2.6	2.6	2.6	2.7	2.6	2.8	3.3	3.4	3.9	5.7	4.6	9.9	12.2	12.6	12.5	15.6	11.3	12.5	11.7	10.3
490 500	2.4	2.3	3.4	2.5	2.4	2.4	1.6	3.0	2.3	2.7	2.3	2.5	2.6	2.5	3.5	3.0	3.3	2.9	4.0	3.9	3.8	5.1	4.2	8.3	10.6	10.5	10.9	12.0	9.3	10.6	8.5	9.5
500 510	2.4	2.0	2.7	2.2	2.3	2.3	1.4	2.7	1.8	2.1	2.1	2.2	2.2	2.2	3.0	3.1	2.8	3.5	3.6	2.9	5.0	3.5	6.7	6.8	7.0	7.4	8.6	7.1	6.9	7.2	7.2	7.6
510 520	2.3	2.2	2.8	2.2	1.8	1.7	1.3	2.1	1.8	2.0	2.0	2.2	2.0	2.7	2.9	2.9	3.7	2.5	2.5	2.6	4.2	3.2	6.1	6.2	6.1	5.7	5.7	4.9	5.3	5.8	5.8	5.3
520 530	2.6	2.3	2.3	2.5	1.9	1.8	1.5	1.9	1.6	1.5	1.9	2.2	2.1	2.0	2.5	2.7	2.6	2.3	3.0	3.8	3.5	4.5	3.0	5.7	6.0	6.1	5.4	4.6	4.6	4.8	4.0	5.4
530 540	2.5	2.3	2.7	2.8	1.9	1.5	1.6	3.0	1.6	2.5	1.8	2.0	2.1	2.2	2.4	2.3	2.2	2.5	3.5	2.8	3.3	3.0	4.1	4.8	5.9	5.7	5.1	4.3	4.0	5.2	4.5	5.5
540 550	2.8	2.5	3.2	3.3	2.1	1.5	1.7	2.6	2.0	2.4	2.2	2.2	2.3	2.5	2.7	3.0	2.7	2.3	3.5	3.1	2.7	2.8	4.3	4.7	4.9	4.9	5.1	4.4	4.1	3.9	4.3	6.0
550 560	3.5	2.7	3.1	3.3	2.2	1.8	2.1	2.4	2.2	2.4	2.3	2.4	2.3	2.7	2.9	3.4	2.9	3.4	4.0	4.0	4.2	5.3	5.1	5.4	6.1	5.6	5.7	5.7	4.8	4.7	6.5	6.5
560 570	3.4	2.5	3.6	3.2	2.5	3.2	3.4	3.3	3.6	3.6	3.7	3.4	3.3	3.4	3.2	3.9	3.7	3.6	4.0	4.6	4.6	5.2	5.0	6.3	5.1	6.0	6.4	5.4	5.6	5.2	5.7	6.8
570 580	3.5	2.7	3.8	2.8	2.5	2.4	3.5	4.8	4.5	4.2	4.1	3.7	4.0	4.1	4.4	4.9	5.3	5.4	5.2	5.0	5.2	5.8	6.0	6.1	7.2	7.0	6.5	6.8	6.8	5.5	6.1	6.8
580 590	3.2	2.8	3.4	2.9	3.1	2.6	3.2	4.5	5.2	4.6	4.6	4.5	4.6	5.2	5.0	4.4	5.0	5.5	6.1	4.9	5.1	5.4	5.3	5.6	5.5	5.9	6.5	5.7	6.4	6.2	6.2	7.6
590 600	3.0	3.1	4.6	4.2	3.3	3.3	3.9	5.0	5.1	5.0	4.6	4.6	4.6	4.5	4.8	4.8	6.3	6.9	7.6	7.2	8.7	8.2	7.0	7.3	7.5	7.3	6.9	6.4	7.9	6.6	7.2	8.0

[a] The wavelength range that gives the lowest averaged absolute percent error is highlighted in a red box. The averaged absolute percent error shown were obtained by comparing *er* and *dr* values collected using LP-generated sensing data against actual values across 20 samples in the training set. Column CD_A denotes the 10 nm wavelength segments of the calibration curves obtained with the Schiff base Cu[II] complexes and row CD_B denotes the 10 nm wavelength segments of the calibration curves obtained with the assemblies in the presence of base. The color scheme in the table shows gradation among the calculated averaged absolute percent error indicating an increase in percent error as it goes from green to red (i.e., values having lowest %error are in green and values having highest percent error are in red).

general protocol. The UV signals between 338 to 345 nm were then fed into the LP algorithm and the concentrations of aminoindanol were calculated with high accuracy in all cases.

Altogether, we have thus demonstrated that our method can be used for comprehensive concentration, *er* and *dr* sensing of aminoindanol samples with strikingly different stereoisomeric compositions. Importantly, our approach is not restricted to this particular amino alcohol but rather generally applicable. Employing 1-amino-2-cyclohexanol as another test analyte in our UV/CD sensing protocol also gave striking CD_A/CD_B signal modulations and diastereoselective UV changes that can be used for *er* and *dr* quantification using the machine learning approach discussed above (Supporting Information).

Conclusion

We have developed a chiroptical sensing method that allows accurate determination of the absolute configuration, enantiomeric composition, diastereomeric ratio, and total amount of a mixture of four stereoisomers using amino-indanol as a test compound. The stereodifferentiation is based on fast Schiff base formation and Cu[II] coordination chemistry that are quantified by simple UV and CD measurements,

which can be performed simultaneously with modern UV/CD instruments and plate readers. All chiroptical signals used for the analysis appear above 300 nm, which is advantageous because this is likely to eliminate possible interferences from impurities that may be present. Our assay exclusively uses inexpensive chemicals, eliminates protection chemistry and any type of sample work-up, and it follows a simple mix-and-measure workflow that is fully adaptable to multiwell plate technology and applicable to microscale analysis. An inert atmosphere and the use of anhydrous solvents are not necessary, and all steps occur in the same solvent at room temperature, which greatly simplifies sample handling and streamlines the operation. LP was used to optimize the weighting of the UV and CD spectra and a PS algorithm enabled unbiased identification of optimal wavelength ranges for the most accurate and robust analysis using 20 training samples. The combination of a powerful sensing assay and supervised learning method proved very efficient, which was demonstrated with the determination of the concentrations and relative amounts of each of the four amino alcohol stereoisomers in 20 samples with an averaged percent error of only 1.7%.

Table 2: Summary of the results obtained from the simultaneous determination of 20 samples containing **1** in varying *er* and *dr* using the wavelength range obtained by PS algorithm (340 to 350 nm for CD_A and 410 to 420 nm for CD_B).

Sample		Conc. (mM) Actual	LP	%Comp. Actual	LP	Absolute Error mM	%	Sample		Conc. (mM) Actual	LP	%Comp. Actual	LP	Absolute Error mM	%
S1	RS	14.6	14.6	73.0	73.1	0.0	0.1	S11	RS	3.0	2.9	15.0	14.3	0.1	0.7
	SR	2.0	2.2	10.0	10.9	0.2	0.9		SR	0.4	0.5	2.0	2.7	0.1	0.7
	RR	2.9	2.6	14.3	13.0	0.3	1.3		RR	13.9	14.3	69.7	71.6	0.4	1.9
	SS	0.5	0.6	2.7	3.0	0.1	0.3		SS	2.7	2.3	13.3	11.4	0.4	1.9
	RS + SR	16.6	16.8	83.0	84.0	0.2	1.0		RS + SR	3.4	3.4	17.0	17.0	0.0	0.0
	RR + SS	3.4	3.2	17.0	16.0	0.2	1.0		RR + SS	16.6	16.6	83.0	83.0	0.0	0.0
S2	RS	1.0	0.6	5.0	3.1	0.4	1.9	S12	RS	2.2	2.7	11.0	13.5	0.5	2.5
	SR	5.2	5.6	26.0	27.9	0.4	1.9		SR	11.6	11.4	58.0	57.2	0.2	0.8
	RR	1.7	1.7	8.3	8.7	0.1	0.4		RR	0.7	0.4	3.7	2.0	0.3	1.7
	SS	12.1	12.1	60.7	60.3	0.1	0.4		SS	5.5	5.5	27.3	27.3	0.0	0.0
	RS + SR	6.2	6.2	31.0	31.0	0.0	0.0		RS + SR	13.8	14.1	69.0	70.7	0.3	1.7
	RR + SS	13.8	13.8	69.0	69.0	0.0	0.0		RR + SS	6.2	5.9	31.0	29.3	0.3	1.7
S3	RS	18.0	18.2	90.2	90.8	0.1	0.6	S13	RS	0.4	0.6	1.8	3.0	0.2	1.2
	SR	1.6	1.6	7.8	8.2	0.1	0.4		SR	0.0	0.2	0.2	3.6	0.7	3.4
	RR	0.4	0.0	1.9	0.0	0.4	1.9		RR	18.2	17.9	91.1	89.6	0.3	1.5
	SS	0.0	0.2	0.1	1.0	0.2	0.9		SS	1.4	0.8	6.9	3.8	0.6	3.1
	RS + SR	19.6	19.8	98.0	99.0	0.2	1.0		RS + SR	0.4	1.3	2.0	6.6	0.9	4.6
	RR + SS	0.4	0.2	2.0	1.0	0.2	1.0		RR + SS	19.6	18.7	98.0	93.4	0.9	4.6
S4	RS	16.4	16.0	81.9	79.8	0.4	2.1	S14	RS	1.6	1.6	8.1	8.1	0.0	0.0
	SR	1.8	2.0	9.1	10.2	0.2	1.1		SR	0.2	0.6	0.9	3.2	0.5	2.3
	RR	1.5	1.6	7.6	7.9	0.1	0.3		RR	15.3	15.5	76.4	77.5	0.2	1.1
	SS	0.3	0.4	1.4	2.1	0.1	0.7		SS	2.9	2.2	14.6	11.2	0.7	3.4
	RS + SR	18.2	18.0	91.0	90.0	0.2	1.0		RS + SR	1.8	2.3	9.0	11.3	0.5	2.3
	RR + SS	1.8	2.0	9.0	10.0	0.2	1.0		RR + SS	18.2	17.7	91.0	88.7	0.5	2.3
S5	RS	12.5	12.7	62.4	63.5	0.2	1.1	S15	RS	3.1	2.8	15.6	13.9	0.3	1.7
	SR	3.5	3.5	17.6	17.5	0.0	0.1		SR	0.9	0.8	4.4	3.9	0.1	0.5
	RR	2.7	2.7	13.6	13.5	0.0	0.1		RR	10.9	11.4	54.4	57.1	0.5	2.7
	SS	1.3	1.1	6.4	5.5	0.2	0.9		SS	5.1	5.0	25.6	25.1	0.1	0.5
	RS + SR	16.0	16.2	80.0	81.0	0.2	1.0		RS + SR	4.0	3.6	20.0	17.8	0.4	2.2
	RR + SS	4.0	3.8	20.0	19.0	0.2	1.0		RR + SS	16.0	16.4	80.0	82.2	0.4	2.2
S6	RS	8.0	8.2	40.0	41.0	0.2	1.0	S16	RS	3.6	3.3	18.0	16.4	0.3	1.6
	SR	5.8	6.2	29.0	31.0	0.4	2.0		SR	2.6	2.9	13.0	14.5	0.3	1.5
	RR	3.5	3.2	17.7	15.9	0.4	1.8		RR	7.9	7.9	39.3	39.3	0.0	0.0
	SS	2.7	2.4	13.3	12.1	0.2	1.2		SS	5.9	6.0	29.7	29.8	0.0	0.1
	RS + SR	13.8	14.4	69.0	72.0	0.6	3.0		RS + SR	6.2	6.2	31.0	30.9	0.0	0.1
	RR + SS	6.2	5.6	31.0	28.0	0.6	3.0		RR + SS	13.8	13.8	69.0	69.1	0.0	0.1
S7	RS	4.6	5.1	22.8	25.6	0.6	2.8	S17	RS	4.0	3.5	20.2	17.5	0.5	2.7
	SR	6.0	5.7	30.2	28.4	0.4	1.8		SR	5.4	5.9	26.8	29.5	0.5	2.7
	RR	3.9	3.4	19.7	17.2	0.5	2.5		RR	4.6	5.3	22.8	26.3	0.7	3.5
	SS	5.5	5.8	27.3	28.8	0.3	1.5		SS	6.1	5.3	30.7	26.7	0.8	4.0
	RS + SR	10.6	10.8	53.0	54.0	0.2	1.0		RS + SR	9.4	9.4	47.0	47.0	0.0	0.0
	RR + SS	9.4	9.2	47.0	46.0	0.2	1.0		RR + SS	10.6	10.6	53.0	53.0	0.0	0.0
S8	RS	2.3	1.6	11.5	8.2	0.7	3.3	S18	RS	4.0	3.9	19.8	19.4	0.1	0.4
	SR	4.9	6.0	24.5	29.8	1.1	5.3		SR	7.0	7.9	35.2	39.6	0.9	4.4
	RR	2.8	2.1	14.1	10.5	0.7	3.6		RR	2.5	2.4	12.6	12.1	0.1	0.5
	SS	10.0	10.3	49.9	51.5	0.3	1.6		SS	6.5	5.8	32.4	28.9	0.7	3.5
	RS + SR	7.2	7.6	36.0	38.0	0.4	2.0		RS + SR	11.0	11.8	55.0	59.0	0.8	4.0
	RR + SS	12.8	12.4	64.0	62.0	0.4	2.0		RR + SS	9.0	8.2	45.0	41.0	0.8	4.0
S9	RS	1.3	1.4	6.5	7.0	0.1	0.5	S19	RS	4.1	4.8	20.5	24.1	0.7	3.6
	SR	3.5	3.2	17.5	16.0	0.3	1.5		SR	11.1	11.1	55.5	55.7	0.0	0.2
	RR	2.9	4.5	14.4	22.4	1.6	8.0		RR	0.9	0.7	4.6	3.7	0.2	0.9
	SS	12.3	10.9	61.6	54.6	1.4	7.0		SS	3.9	3.3	19.4	16.5	0.6	2.9
	RS + SR	4.8	4.6	24.0	23.0	0.2	1.0		RS + SR	15.2	16.0	76.0	79.8	0.8	3.8
	RR + SS	15.2	15.4	76.0	77.0	0.2	1.0		RR + SS	4.8	4.0	24.0	20.2	0.8	3.8
S10	RS	0.5	0.7	2.4	3.3	0.2	0.9	S20	RS	2.7	3.0	13.6	15.0	0.3	1.4
	SR	2.5	2.5	12.6	12.7	0.0	0.1		SR	14.3	14.3	71.4	71.6	0.0	0.2
	RR	1.7	1.0	8.5	4.9	0.7	3.6		RR	0.3	0.0	1.5	0.0	0.3	1.5
	SS	15.3	15.8	76.5	79.1	0.5	2.6		SS	2.7	2.7	13.5	13.4	0.0	0.1
	RS + SR	3.0	3.2	15.0	16.0	0.2	1.0		RS + SR	17.0	17.3	85.0	86.6	0.3	1.6
	RR + SS	17.0	16.8	85.0	84.0	0.2	1.0		RR + SS	3.0	2.7	15.0	13.4	0.3	1.6

Sample	Actual values (mM)	Sensing results (LP) (mM)	Absolute error (mM)
S21	15.0	15.1	0.1
S22	10.0	10.0	0.0
S23	16.6	17.6	1.0
S24	13.6	15.1	1.5
S25	11.8	12.0	0.2
S26	8.4	8.1	0.3
S27	6.0	7.2	1.2
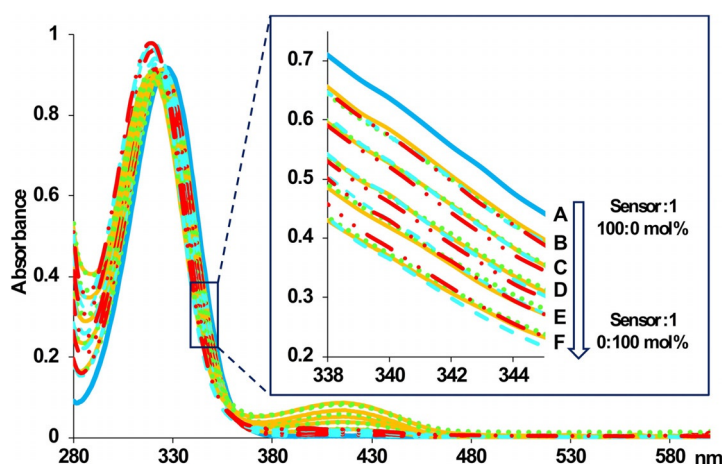
Figure 4. Left: UV/Vis spectra of the salicylaldimine formed with increasing concentration of **1**. Inset: As the concentration of **1** increases, a concomitant hypsochromic shift and a decrease in signal intensity are observed. UV/Vis analysis was performed at a concentration of 0.2 mM in DMSO. Note that in the region between 338 to 345 nm, the imines formed from the enantiomers and diastereomers of **1** produce superimposable responses which allows concentration determination of the analyte. A = 0 mol % **1**, B = 20 mol % **1**, C = 40 mol % **1**, D = 60 mol % **1**, E = 80 mol % **1**, F = 100 mol % **1**. Blue curve = sensor **2**, orange = (R,S)-**1**, green = (S,R)-**1**, cyan = (R,R)-**1** and red: = (S,S)-**1**. Right: Concentration determination of seven samples of **1**.

Conflict of interest

The authors declare no conflict of interest.

Keywords: chirality sensing · circular dichroism · machine learning · stereoisomer analysis · UV spectroscopy

[1] a) D. W. Robbins, J. F. Hartwig, *Science* **2011**, *333*, 1423–1427; b) A. McNally, C. K. Prier, D. W. C. MacMillan, *Science* **2011**, *334*, 1114–1117; c) A. Buitrago Santanilla, E. L. Regalado, T. Pereira, M. Shevlin, K. Bateman, L. C. Campeau, J. Schneeweis, S. Berritt, Z.-C. Shi, P. Nantermet, Y. Liu, R. Helmy, C. J. Welch, P. Vachal, I. W. Davies, T. Cernak, S. D. Dreher, *Science* **2015**, *347*, 49–53.

[2] K. D. Collins, T. Gensch, F. Glorius, *Nat. Chem.* **2014**, *6*, 859–871.

[3] a) C. J. Welch, *Chirality* **2009**, *21*, 114–118; b) D. D. Kotoni, A. Ciogli, C. Molinaro, I. D'Acquarica, J. Kocergin, T. Szczerba, H. Ritchie, C. Villani, F. Gasparrini, *Anal. Chem.* **2012**, *84*, 6805–6813; c) D. C. Patel, F. M. Wahab, D. W. Armstrong, Z. S. Breitbach, *J. Chromatogr. A* **2016**, *1467*, 2–18; d) C. L. Barhate, L. A. Joyce, A. A. Makarov, K. Zawatzky, F. Bernardoni, W. A. Schafer, D. W. Armstrong, C. J. Welch, E. L. Regalado, *Chem. Commun.* **2017**, *53*, 509–512.

[4] a) J. Guo, J. Wu, G. Siuzdak, M. G. Finn, *Angew. Chem. Int. Ed.* **1999**, *38*, 1755–1758; *Angew. Chem.* **1999**, *111*, 1868–1871; b) M. T. Reetz, M. H. Becker, H.-W. Klein, D. Stockigt, *Angew. Chem. Int. Ed.* **1999**, *38*, 1758–1761; *Angew. Chem.* **1999**, *111*, 1872–1875; c) C. Markert, A. Pfaltz, *Angew. Chem. Int. Ed.* **2004**, *43*, 2498–2500; *Angew. Chem.* **2004**, *116*, 2552–2554; d) C. A. Müller, C. Markert, A. M. Teichert, A. Pfaltz, *Chem. Commun.* **2009**, 1607–1618; e) C. Ebner, C. A. Muller, C. Markert, A. Pfaltz, *J. Am. Chem. Soc.* **2011**, *133*, 4710–4713; f) S. Piovesana, R. Samperi, A. Laganà, M. Bella, *Chem. Eur. J.* **2013**, *19*, 11478–11494.

[5] a) M. T. Reetz, M. H. Becker, K. M. Kuhling, A. Holzwarth, *Angew. Chem. Int. Ed.* **1998**, *37*, 2647–2650; *Angew. Chem.* **1998**, *110*, 2792–2795; b) P. Tielmann, M. Boese, M. Luft, M. T. Reetz, *Chem. Eur. J.* **2003**, *9*, 3882–3887.

[6] a) M. T. Reetz, A. Eipper, P. Tielmann, R. Mynott, *Adv. Synth. Catal.* **2002**, *344*, 1008–1016; b) M. A. Evans, J. P. Morken, *J. Am. Chem. Soc.* **2002**, *124*, 9020–9021; c) M.-S. Seo, H. Kim, *J. Am. Chem. Soc.* **2015**, *137*, 14190–14195; d) Y. Zhao, T. M. Swager, *J. Am. Chem. Soc.* **2015**, *137*, 3221–3224; e) H. Huang, G. Bian, H. Zong, Y. Wang, S. Yang, H. Yue, L. Song, H. Fan, *Org. Lett.* **2016**, *18*, 2524–2527; f) L. Yang, T. Wenzel, R. T. Williamson, M. Christensen, W. Schafer, C. J. Welch, *ACS Cent. Sci.* **2016**, *2*, 332–340; g) G. Bian, S. Yang, H. Huang, H. Zong, L. Song, H. Fan, X. Sun, *Chem. Sci.* **2016**, *7*, 932–938; h) G. Storch, M. Haas, O. Trapp, *Chem. Eur. J.* **2017**, *23*, 5414; i) Q. H. Luu, K. G. Lewis, A. Banerjee, N. Bhuvanesh, J. A. Gladysz, *Chem. Sci.* **2018**, *9*, 5087.

[7] M. T. Reetz, K. M. Kuhling, A. Deege, H. Hinrichs, D. Belder, *Angew. Chem. Int. Ed.* **2000**, *39*, 3891–3893; *Angew. Chem.* **2000**, *112*, 4049–4052.

[8] a) P. Abato, C. T. Seto, *J. Am. Chem. Soc.* **2001**, *123*, 9206–9207; b) F. Taran, C. Gauchet, B. Mohar, S. Meunier, A. Valleix, P. Y. Renard, C. Creminon, J. Grassi, A. Wagner, C. Mioskowski, *Angew. Chem. Int. Ed.* **2002**, *41*, 124–127; *Angew. Chem.* **2002**, *114*, 132–135; c) M. Matsushita, K. Yoshida, N. Yamamoto, P. Wirsching, R. A. Lerner, K. D. Janda, *Angew. Chem. Int. Ed.* **2003**, *42*, 5984–5987; *Angew. Chem.* **2003**, *115*, 6166–6169; d) S. Dey, D. R. Powell, C. Hu, D. B. Berkowitz, *Angew. Chem. Int. Ed.* **2007**, *46*, 7010–7014; *Angew. Chem.* **2007**, *119*, 7140–7144; e) J. A. Friest, S. Broussy, W. J. Chung, D. B. Berkowitz, *Angew. Chem. Int. Ed.* **2011**, *50*, 8895–8899; *Angew. Chem.* **2011**, *123*, 9057–9061; f) F. Biedermann, W. M. Nau, *Angew. Chem. Int. Ed.* **2014**, *53*, 5694–5699; *Angew. Chem.* **2014**, *126*, 5802–5807; g) T. A. Feagin, D. P. V. Olsen, Z. C. Headman, J. M. Heemstra, *J. Am. Chem. Soc.* **2015**, *137*, 4198–4206.

[9] a) G. A. Korbel, G. Lalic, M. D. Shair, *J. Am. Chem. Soc.* **2001**, *123*, 361–362; b) L. Pu, *Chem. Rev.* **2004**, *104*, 1687–1716; c) D. Leung, S. O. Kang, E. V. Anslyn, *Chem. Soc. Rev.* **2012**, *41*, 448–479; d) C. Wolf, K. W. Bentley, *Chem. Soc. Rev.* **2013**, *42*, 5408–5424; For a recent Perspective on this topic: e) B. T. Herrera, S. L. Pilicer, E. V. Anslyn, L. A. Joyce, C. Wolf, *J. Am. Chem. Soc.* **2018**, *140*, 10385–10401.

[10] a) T. D. James, K. R. A. S. Sandanayake, S. Shinkai, *Nature* **1995**, *374*, 345–347; b) X. Mei, C. Wolf, *J. Am. Chem. Soc.* **2004**, *126*, 14736–14737; c) C. Wolf, S. L. Liu, B. C. Reinhardt, *Chem. Commun.* **2006**, 4242–4244; d) X. Mei, C. Wolf, *J. Am. Chem. Soc.* **2006**, *128*, 13326–13327; e) X. He, Q. Zhang, X. Liu, L. Lin, X. Feng, *Chem. Commun.* **2011**, *47*, 11641–11643; f) S. Yu, L. Pu, *J. Am. Chem. Soc.* **2010**, *132*, 17698–17700; g) S. Yu, W. Plunkett, M. Kim, L. Pu, *J. Am. Chem. Soc.* **2012**, *134*, 20282–20285; h) K. Wen, S. Yu, Z. Huang, L. Chen, M. Xiao, X. Yu, L. Pu, *J. Am. Chem. Soc.* **2015**, *137*, 4517–4524; i) A. Akdeniz, L. Mosca, T. Minami, P. Anzenbacher, Jr., *Chem. Comm.* **2015**, *51*, 5770–5773; j) E. G. Shcherbakova, T. Minami, V. Brega, T. D. James, P. Anzenbacher, Jr., *Angew. Chem. Int. Ed.* **2015**, *54*, 7130–7133; *Angew. Chem.* **2015**, *127*, 7236–7239; k) A. Akdeniz, T. Minami, S. Watanabe, M. Yokoyama, T. Ema, P. Anzenbacher, Jr., *Chem. Sci.* **2016**, *7*, 2016–2022; l) L. Pu, *Acc. Chem. Res.* **2017**, *50*, 1032–1040.

[11] a) L. Zhu, E. V. Anslyn, *J. Am. Chem. Soc.* **2004**, *126*, 3676–3677.

[12] a) L. Zhu, S. H. Shabbir, E. V. Anslyn, *Chem. Eur. J.* **2007**, *13*, 99–104; b) P. Zhang, C. Wolf, *Chem. Commun.* **2013**, *49*, 7010–7012; c) K. W. Bentley, C. Wolf, *J. Am. Chem. Soc.* **2013**, *135*, 12200–12203; d) P. Zardi, K. Wurst, G. Licini, C. Zonta, *J. Am. Chem. Soc.* **2017**, *139*, 15616; e) F. Y. Thanzeel, C. Wolf, *Angew. Chem. Int. Ed.* **2017**, *56*, 7276–7281; *Angew. Chem.* **2017**, *129*, 7382–7387.

[13] a) S. H. Shabbir, J. R. Clinton, E. V. Anslyn, *Proc. Natl. Acad. Sci. USA* **2009**, *106*, 10487–10492; b) S. Nieto, J. M. Dragna, E. V. Anslyn, *Chem. Eur. J.* **2010**, *16*, 227–232; c) K. W. Bentley, D. Proano, C. Wolf, *Nat. Commun.* **2016**, *7*, 12539; d) E. G. Shcherbakova, V. Brega, V. M. Lynch, T. D. James, P. Anzenbacher, *Chem. Eur. J.* **2017**, *23*, 10222–10229; e) K. W. Bentley, P. Zhang, C. Wolf, *Sci. Adv.* **2016**, *2*, e1501162; f) M. W. Giuliano, C. Y. Lin, D. K. Romney, S. J. Miller, E. V. Anslyn, *Adv. Synth. Catal.* **2015**, *357*, 2301–2309; g) Z. A. De los Santos, C. Wolf, *J. Am. Chem. Soc.* **2016**, *138*, 13517–13520; h) L. A. Joyce, E. C. Sherer, C. J. Welch, *Chem. Sci.* **2014**, *5*, 2855–2861; i) F. Y. Thanzeel, K. Balaraman, C. Wolf, *Nat. Commun.* **2018**, *9*, 5323.

[14] S. Nieto, V. M. Lynch, E. V. Anslyn, H. Kim, J. Chin, *J. Am. Chem. Soc.* **2008**, *130*, 9232–9233.

[15] D. P. Iwaniuk, K. Yearick-Spangler, C. Wolf, *J. Org. Chem.* **2012**, *77*, 5203–5208.

[16] S. S. Yu, L. Pu, *Sci. China Chem.* **2013**, *56*, 301–306.

[17] B. T. Herrera, S. R. Moor, M. McVeigh, E. K. Roesner, F. Marini, E. V. Anslyn, *J. Am. Chem. Soc.* **2019**, *141*, 11151–11160.

[18] C. Wolf, *Dynamic Stereochemistry of Chiral Compounds*, RSC Publishing, Cambridge, **2008**, pp. 136–179.

[19] a) S. L. Pilicer, P. R. Bakhshi, K. W. Bentley, C. Wolf, *J. Am. Chem. Soc.* **2017**, *139*, 1758–1761; b) S. L. Pilicer, M. Mancinelli, A. Mazzanti, C. Wolf, *Org. Biomol. Chem.* **2019**, *17*, 6699–6705.

[20] a) K. W. Bentley, Y. G. Nam, J. M. Murphy, C. Wolf, *J. Am. Chem. Soc.* **2013**, *135*, 18052–18055; b) Z. A. De los Santos, L. A. Joyce, E. C. Sherer, C. J. Welch, C. Wolf, *J. Org. Chem.* **2019**, *84*, 4639–4645.

[21] a) Z. A. De los Santos, C. C. Lynch, C. Wolf, *Angew. Chem. Int. Ed.* **2019**, *58*, 1198–1202; *Angew. Chem.* **2019**, *131*, 1211–1215; b) C. C. Lynch, Z. A. De los Santos, C. Wolf, *Chem. Commun.* **2019**, *55*, 6297–6300.

[22] Selected examples: a) M. Biswas, G. Pilet, J. Tercero, M. S. El Fallah, S. Mitra, *Inorg. Chim. Acta* **2009**, *362*, 2915–2920; b) V. Chandrasekhar, T. Senapati, A. Dey, E. C. Sanudo, *Inorg. Chem.* **2011**, *50*, 1420–1428; c) S. Ding, Y. Gao, Y. Ji, Y. Wang, Z. Liu, *CrystEngComm* **2013**, *15*, 5598–5601; d) S. Dasgupta, I. Majumder, P. Chakraborty, E. Zangrando, A. Bauza, A. Frontera, D. Das, *Eur. J. Inorg. Chem.* **2017**, 133–145; e) K. Peewasan, M. P. Merkel, K. Zarschler, H. Stephan, C. E. Anson, A. K. Powell, *RSC Adv.* **2019**, *9*, 24087–24091.

[23] a) T. Aratani, Y. Toneyoshi, T. Nagase, *Tetrahedron Lett.* **1975**, *16*, 1707–1710; b) A. Aratani, *Pure Appl. Chem.* **1985**, *57*, 1839–1844; c) C. Jiang, Z. Ming, Q. Tan, D. Qian, T. You, *Enantiomer* **2002**, *7*, 287–293; d) G. Desimoni, G. Dusi, G. Faita, P. Quadrelli, P. P. Righetti, *Tetrahedron* **1995**, *51*, 4131–4144; e) M. Itagaki, K. Hagiya, M. Kamitamari, K. Masumoto, K. Suenobu, Y. Yamamoto, *Tetrahedron* **2004**, *60*, 7835–7843.

[24] CCDC 1953287 and 1953286 contains the supplementary crystallographic data for this paper. These data can be obtained free of charge from The Cambridge Crystallographic Data Centre.